

The Onset of Temperature Chaos

Hongze Li, Jiaming He, and Raymond L. Orbach

Texas Materials Institute, The University of Texas at Austin, Austin, Texas 78712, USA

(Dated: November 21, 2024)

Temperature chaos (TC) in spin glasses has been claimed to exist no matter how small the temperature change, ΔT . However, experimental studies have exhibited a finite value of ΔT for a transition to TC. This paper explores the onset of TC with much higher resolution than before and over a larger temperature range. We find that TC is always present, though small at the smallest ΔT that we can reliably measure. However, it grows rapidly as ΔT increases, the region of rapid growth coinciding with the ΔT predicted from renormalization group arguments and observed experimentally. We are able to transcend the full range of TC, from reversible (TC = 0) to fully chaotic (complete TC).

I. INTRODUCTION

Temperature chaos (TC) in spin glasses has been controversial ever since it was first introduced [1–4]. The simplest description of TC is “...the complete reorganization of the equilibrium configurations by the slightest change in temperature” [5]. Concomitantly, extending the analysis to off-equilibrium dynamics, TC “...means that the spin configurations that are typical from the Boltzmann weight at temperature T_1 [we refer below to this temperature as T_{initial}] are very atypical at temperature T_2 [we refer below to this temperature as T_{final}] no matter how close the two temperatures T_1 and T_2 are” [6]. A rather complete listing of theoretical papers, supporting or questioning the existence of TC, can be found in [7]. Experimentally, the three experimental papers that have reported TC in spin glasses, [7–9], observe the onset of TC only at a relatively large temperature change, close to that predicted from renormalization group arguments [1, 2].

This paper probes the presence of TC at a higher level of resolution, and exhibits TC for even the smallest $\Delta T = T_{\text{initial}} - T_{\text{final}}$ we can reliably measure. We find its magnitude to be small at the smallest temperature change, ΔT , resolving the apparent contradiction between theory and experiment. TC does become large at a crossover temperature close to that predicted from renormalization group arguments [1, 2], and in the range of ΔT reported in the previous experimental reports [7–9]. We find TC to continue to increase with increasing ΔT until the entirety of the spin glass system is in a chaotic state.

Previous work [10, 11] has quantitatively described the nature of TC in spin glasses. Their analysis begins with the preparation of the spin glass at some initial temperature, T_{initial} . The spin glass is aged for a time $t_{w,\text{initial}}$ allowing the growth of the correlation length from nucleation to $\xi(t_{w,\text{initial}}, T_{\text{initial}})$. Next, the temperature is dropped to T_{final} and the spin glass is aged for $t_{w,\text{final}}$, allowing a new correlation length to grow from nucleation to $\xi(t_{w,\text{final}}, T_{\text{final}})$. Because of the rapid slowing down of the growth of the spin glass correlation length with decreasing temperature [12–14], the correlations created

at T_{initial} are essentially frozen at T_{final} . The associated correlated volume, subtended by $\xi(t_{w,\text{initial}}, T_{\text{initial}})$, interferes with the growth of $\xi(t_{w,\text{final}}, T_{\text{final}})$, leading to quantitative predictions for rejuvenation and the magnitude of memory. The reader is referred to [10, 11] for full details. The basic assumption underlying their analysis, and our own below, is that TC results from an *independent* growth of a chaotic regime at T_{final} .

Our investigation focuses on when TC first appears. We do three independent experiments. First, we cool the spin glass from above T_g , the spin glass transition temperature, to an initial temperature T_{initial} and age the system for a time $t_{w,\text{initial}}$. We lower the temperature (as rapidly as possible) to T_{final} and age again for $t_{w,\text{final}}$. We apply a magnetic field, and measuring the time dependence of the (slowly) increasing magnetization, from which we extract an effective response time $t_{w,T_{\text{initial}} \rightarrow T_{\text{final}}}^{\text{eff}}$ (see below for the details). Second, we start over, drop the temperature from above T_g to T_{initial} , age for $t_{w,\text{initial}}$, turn on the magnetic field, and measure the effective response time $t_{w,\text{initial}}^{\text{eff}}$. We then calculate what that effective response time would be at T_{final} which we refer to as $t_{w,r}^{\text{eff}}$ (again, see below for the details). Third, we start over, drop the temperature from above T_g to T_{final} , age for $t_{w,\text{final}}$, turn on the magnetic field, and measure the effective response time $t_{w,\text{final}}^{\text{eff}}$ which, for purposes of notation, we call $t_{w,\text{native}}^{\text{eff}}$. The sum of $t_{w,r}^{\text{eff}}$ and $t_{w,\text{native}}^{\text{eff}}$ is labeled $t_{w,R}^{\text{eff}}$, where r and R refer to reversible behavior. If $t_{w,T_{\text{initial}} \rightarrow T_{\text{final}}}^{\text{eff}} = t_{w,R}^{\text{eff}}$, there is no TC. If $t_{w,T_{\text{initial}} \rightarrow T_{\text{final}}}^{\text{eff}} < t_{w,R}^{\text{eff}}$, TC is present, the relative amount of which is the difference between the two effective response times.

In ordinary words, there is no TC when the cycled system has the same effective response time as the initially prepared system when cooled to T_{final} . However, if the effective response time of the cycled system is less than the initially prepared system when cooled to T_{final} , then there has been interference in the cycling process, reducing the effective response time, and concomitantly, reducing the correlation length of the cycled system. We associate this interference with TC. The *amount* of reduction is a direct measure of the amount of TC. Below, we present the specific details underlying the above anal-

ysis. We will work with the same sample (single crystal CuMn, 6 at.%, $T_g = 31.5$ K) at the same waiting time ($t_{w,\text{initial}} = 10^4$ s) employed by [7] in order to be sure that we are in a temperature and time range that has been previously reported for the onset of TC.

II. EXPERIMENTAL PROTOCOL

The method we use relies on extracting the characteristic response time defined as the time when the relaxation function

$$S(t) = dM(t, t_w; H)/d\ln t \quad (1)$$

peaks from time dependent magnetization measurements. This time, termed t_w^{eff} , is close to the impressed waiting time t_w , and has been the standard means of extracting the response time for spin glass dynamics ever since it was introduced by Nordblad et al. [15]. It was used, as an example, by Joh et al. [16] to measure the shift of t_w^{eff} with magnetic field in order to extract the spin glass correlation length. The plot of $S(t)$ vs t from Joh et al. [16], for different magnetic fields, is reproduced in Fig. 1.

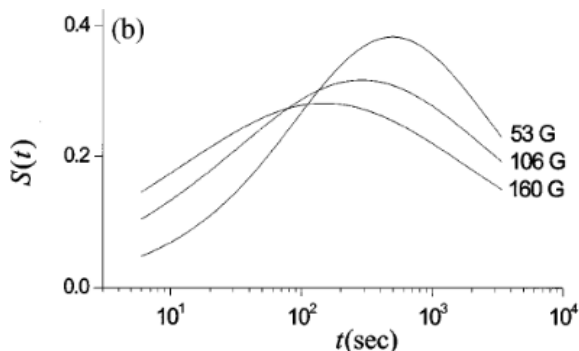


FIG. 1. A plot of $S(t)$, defined in Eq. (1), vs t for different values of magnetic field for a CuMn 6 at.% polycrystalline sample. Note that the width of the $S(t)$ curves may make it difficult to extract the precise position of the peak time. Reproduced from Fig. 1b of Ref. [16].

Some representative plots of $S(t)$ for our single crystal CuMn 6 at.% sample can be found in Appendix A, Figs. 7 and 9. The width of the $S(t)$ curve as a function of time t makes it difficult to extract a precise value for the time at which $S(t)$ peaks. Our method for achieving the necessary accuracy is described in Appendix A. We also check magnetic field linearity in Appendix B.

The extracted t_w^{eff} produces an important physical quantity. The magnitude of the largest free energy barrier, $\Delta_{\text{max}}(t_w, T)$, generated by the growth of the spin glass correlation length, is connected to t_w^{eff} through an Arrhenius relation,

$$t_w^{\text{eff}} = \tau_0 \exp[\Delta_{\text{max}}(t_w, T)/k_B T], \quad (2)$$

where τ_0 is a typical exchange time, usually taken as $\tau_0 = \hbar/k_B T_g$. This relationship is based on a hierarchical organization of metastable states, first articulated by Refregier et al. [17]. Subsequent analysis [18, 19] gave relevance of this structure to that of Parisi’s solution [20, 21] of the Sherrington-Kirkpatrick mean-field model [22]. A more recent publication, “Real Spin Glasses Relax Slowly in the Shade of Hierarchical Trees” [23] is particularly convincing in this respect.

Parisi’s solution was expressed in terms of his “pure states” which are separated from one another by infinite barriers. As a consequence, there are no dynamics arising from these states. Experiments [19, 23] demonstrated a self-similarity structure for states separated by finite free energy barriers. Going further, Hammann et al [19] found a strong temperature dependence for the barrier heights, displayed in Fig. 2. The remarkable feature of Fig. 2 is that the data are *independent* of temperature, and can be fitted, with equally acceptable results, to a power law

$$-d\Delta/dT_r = a\Delta^n, \quad (3)$$

with $a = 2.9 \times 10^{-7}$ and $n = 6$, as shown by the dashed line in Fig. 2, or to an exponential form,

$$-d\Delta/dT_r = \alpha \exp(\beta\Delta), \quad (4)$$

with $\alpha = 0.5$ and $\beta = 0.2$ [19]. Integration of Eq. (3) and Eq. (4) generates diverging barrier heights for decreasing temperature:

$$\Delta(T) = [a(n-1)(T-T^*)/T_g]^{1/(1-n)} \quad (5)$$

and

$$\Delta(T) = -(1/\beta) \ln[\alpha\beta(T-T^*)/T_g] \quad (6)$$

where $T > T^*$ and $n > 1$. The temperature T^* , where the barrier heights diverge, arises from the integration constant.

It is useful to plot Δ in units of T_g against $dT = (T-T^*)/T_g$ as shown in Fig. 3 for the exponential fit Eq. (4). There are two features of Figs. 2 and 3 that are crucial for our analysis. First, from Fig. 2, no matter what the temperature is (within the experimental range), the relationship between $d\Delta/dT$ and Δ remains the same. We interpret this to mean that the states accessed at different temperatures are self-similar: their structure does not change with temperature. Second, from Fig. 3, the barrier heights become very large as the temperature approaches T^* from above. Said another way, given a value of Δ at a temperature T , then as T is reduced, Δ becomes very large as T approaches T^* .

The point of the above paragraph is that the structure of the Parisi solution of the Sherrington-Kirkpatrick mean field model, with infinite barriers separating “pure states”, is mirrored experimentally in the rapid growth

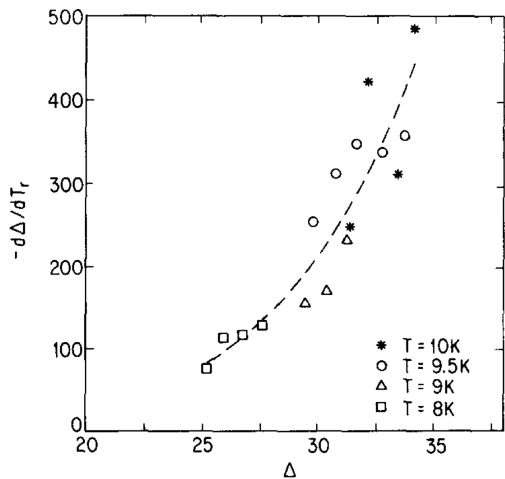


FIG. 2. A plot of $d\Delta/dT_r$ vs Δ in units of T_g , where $T_r = T/T_g$, for each of four values of T , for a Ag:Mn 2.6 at.% sample. The set of data points define a unique curve [the dashed line, Eq. (3)], the points at each fixed value of T are consistent with this unique curve, and the curve is therefore independent of temperature. Reproduced from Fig. 4 of Ref. [19]

of Δ as the temperature is reduced towards T^* , *independent* of the initial temperature T . That is, from experiment, a self-similar set of finite barriers grow very large as $T \rightarrow T^*$, suggesting an experimental analog to Parisi's pure states. The hierarchical structure of the Parisi solution (ultrametric symmetry) is mirrored in the experimental observation of a distribution of finite barriers lying between states of very high barriers. Interpretation of experimental results (e.g. [19] and [17]), and many others up to the present, have used this perspective. As a consequence, growth of the spin glass correlation length $\xi(t_w, T)$ generates growth of Δ (e.g. see Ref. [16]). Furthermore, because ultrametric symmetry leads to an exponential increase in the number of available states with increasing $\xi(t_w, T)$ (concomitantly, increasing Δ), magnetization dynamics are controlled by the *largest* Δ generated through the growth of $\xi(t_w, T)$.

Our experimental procedure is as follows. First, we start the process by cooling from above T_g directly to T_{initial} , and age for a time $t_w = 10^4$ s. We then turn on the magnetic field and measure the time at which $S(t)$ peaks, generating $t_{w,\text{native}}^{\text{eff}}$ at T_{initial} . Second, we repeat this process, but now cool to a set of temperatures $T_{\text{final}} < T_{\text{initial}}$, age for $t_{w,\text{final}} = 10^4$ s, and obtain the time at which $S(t)$ peaks, $t_{w,\text{native}}^{\text{eff}}$ for this set of T_{final} . From the first step, using Eq. (2), we extract $\Delta_{\text{max}}(t_{w,\text{initial}}, T_{\text{initial}})$ from $t_{w,\text{native}}^{\text{eff}}$ at T_{initial} . We then use the extrapolation of Fig. 2 to calculate $\Delta_{\text{max}}(t_{w,\text{final}}, T_{\text{final}})$, which, through Eq. (2), gives a reversible effective response time $t_{w,r}^{\text{eff}}$ at T_{final} . We add $t_{w,\text{native}}^{\text{eff}}$ at T_{final} to the calculated $t_{w,r}^{\text{eff}}$ to generate the quantity t_R^{eff} for each of the values of T_{final} . Finally, we

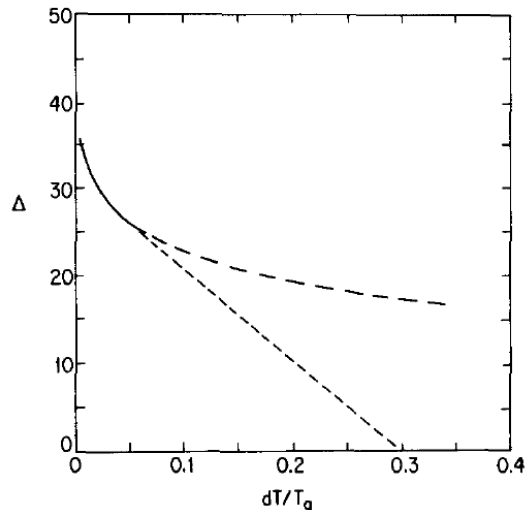


FIG. 3. Using Eq. (4), Δ in units of T_g is plotted against $dT = (T - T^*)/T_g$. The curve (solid line + long dashes) corresponds to Eq. (6), the exponential form. The solid line corresponds to the actual measurements (i.e. lies within the accessible time range). The straight line (short dashes) is an extrapolation to $\Delta = 0$ given by the tangent to the solid line (experimental measurements) at the smallest value of Δ probed experimentally. It gives the minimum temperature range for a barrier to grow from zero to infinity: $dT/T_g = 0.3$. Reproduced from Fig. 5 of Ref. [19].

cool the sample from above T_g to T_{initial} , age for $t_w = 10^4$ s, then cool the sample to T_{final} , and age for $t_w = 10^4$ s. The magnetic field is applied, and $S(t)$ is measured, with its peak time equaling $t_{w,T_{\text{initial}} \rightarrow T_{\text{final}}}^{\text{eff}}$. If $t_R^{\text{eff}} = t_{w,T_{\text{initial}} \rightarrow T_{\text{final}}}^{\text{eff}}$ there is no TC going from T_{initial} to T_{final} . If the two are not equal, the difference $t_R^{\text{eff}} - t_{w,T_{\text{initial}} \rightarrow T_{\text{final}}}^{\text{eff}}$ is the amount of the chaotic component present in the transition from T_{initial} to T_{final} . We present our experimental results, and our analysis, below.

III. MEASUREMENTS AND ANALYSIS

The spin glass CuMn single crystal sample (6 at.% Mn, $T_g = 31.5$ K) is cooled from above T_g to $T_{\text{initial}} = 18.00$ K, a magnetic field of $H = 100$ Oe is applied after an aging time of 10^4 s, and the magnetization change with time recorded. $S(t)$ is created from Eq. (1), and the characteristic response time $t_{w,\text{native}}^{\text{eff}}$ is extracted from the time at which $S(t)$ peaks. It is listed in the first row, second column, of Table I. Its value, using the Arrhenius relation of Eq. (2), generates $\Delta_{\text{max}} = 22.21 T_g$. We then follow the same procedure for a series of temperatures T_{final} , from $T_{\text{final}} = 17.95$ K to as low as $T_{\text{final}} = 6.00$ K. The values for $t_{w,\text{native}}^{\text{eff}}$ for each T_{final} are listed in column 2 of Table I.

The spin glass single crystal sample is now cooled from above T_g to $T_{\text{initial}} = 18.00$ K. The system is aged at

TABLE I. Listing of measured and calculated values for the temperature T_{final} (column 1); the measured native effective response time at T_{final} for $t_{w,\text{initial}} = 10^4$ s (column 2); the measured effective response time after $t_{w,\text{initial}} = 10^4$ s at T_{initial} , dropping the temperature to T_{final} , and waiting for $t_{w,\text{final}} = 10^4$ s (column 3); the calculated effective response time of the reversible (cumulative) portion (column 4); and the calculated native correlation length with $t_{w,\text{initial}} = 10^4$ s (column 5). Our calculations use the power law form, Eq. (3), for the temperature dependence of Δ .

T (K)	$t_{w,\text{native}}^{\text{eff}} (\times 10^4 \text{ s})$	$t_{w,T_{\text{initial}} \rightarrow T_{\text{final}}}^{\text{eff}} (\times 10^4 \text{ s})$	$t_{\text{R}}^{\text{eff}}(\text{s})$	ξ/a_0
18.00	1.84 ± 0.04	-	-	9.715
17.95	1.85 ± 0.02	3.92 ± 0.01	4.10×10^4	9.653
17.90	1.90 ± 0.02	4.38 ± 0.06	4.67×10^4	9.593
17.80	1.90 ± 0.03	5.42 ± 0.10	6.10×10^4	9.472
17.70	1.91 ± 0.02	6.16 ± 0.02	8.31×10^4	9.353
17.55	1.81 ± 0.01	9.21 ± 0.06	1.40×10^5	9.178
17.50	1.89 ± 0.05	10.04 ± 0.03	1.70×10^5	9.120
17.30	1.87 ± 0.02	13.23 ± 0.05	3.81×10^5	8.708
17.00	1.84 ± 0.01	10.68 ± 0.36	1.42×10^6	8.387
16.50	2.00 ± 0.06	5.08 ± 0.04	1.49×10^7	7.722
16.00	1.92 ± 0.01	2.78 ± 0.05	1.83×10^8	7.258
15.50	1.90 ± 0.03	1.90 ± 0.03	2.66×10^9	6.695
15.00	1.89 ± 0.01	1.73 ± 0.02	4.60×10^{10}	6.183
14.50	1.94 ± 0.03	1.66 ± 0.01	9.70×10^{11}	5.717
14.00	2.09 ± 0.01	1.77 ± 0.02	2.54×10^{13}	5.384
13.00	1.84 ± 0.07	1.53 ± 0.02	3.71×10^{16}	4.625
12.00	1.87 ± 0.03	1.59 ± 0.03	1.82×10^{20}	4.052
11.00	1.82 ± 0.01	1.51 ± 0.05	4.20×10^{24}	3.558
6.00	1.62 ± 0.04	1.30 ± 0.01	1.78×10^{68}	1.913

T_{initial} for 10^4 s, the temperature is dropped to T_{final} , and the system is aged for another 10^4 s. After the second aging, a magnetic field of 100 Oe is applied, and the magnetization change is recorded as a function of time. The $S(t)$ curves are generated through Eq. (1), and the effective response times, $t_{w,T_{\text{initial}} \rightarrow T_{\text{final}}}^{\text{eff}}$ for each T_{final} are extracted from the time at which the respective $S(t)$ peaks. Their values are listed in column 3 of Table I. If the system is completely chaotic at a given T_{final} , the values $t_{w,\text{native}}^{\text{eff}}$ (column 2) should be equal to $t_{w,T_{\text{initial}} \rightarrow T_{\text{final}}}^{\text{eff}}$ (column 3). Examination of Table I shows that this occurs for $T_{\text{final}} = 15.50$ or $\Delta T = 2.50$ K. The latter is slightly smaller than the former for all larger ΔT for reasons that will be discussed below. The results of these two procedures are plotted against T_{final} in Fig. 4(a).

The next step is to disentangle the contribution to the measured effective response times reported in column 3 of Table I from the reversible and chaotic components. The native response time at $T_{\text{initial}} = 18.00$ K is the starting point, as no temperature change has occurred, hence no TC. The maximum barrier height, Δ_{max} , is generated by the growth of the correlation length during the aging time $t_w = 10^4$ s at 18.00 K. Naïvely, one might choose to use the Arrhenius relation to calculate the reversible (cumulative) effective response time for each T_{final} . However, that would be incorrect. Hammann et al. [19] showed that Δ_{max} *increases* at the temperature is reduced. They evaluated $d\Delta_{\text{max}}/dT_r$ ($T_r = T/T_g$) as a function of temperature T . We reproduced their findings in Fig. 2 (their $T \equiv T_{\text{initial}}$). We use Fig. 2 to calculate $\Delta_{\text{max}}(t_w, T_{\text{initial}} \rightarrow T_{\text{final}})$ for our CuMn 6 at% spin glass

sample. Though Fig. 2 was for a AgMn sample, their use of reduced units suggests that we can apply it to our CuMn sample.

We attribute the difference between the value of the reversible effective response time, $t_{\text{R}}^{\text{eff}}$, column 4 of Table I, and the experimental value of the cycled effective response time, $t_{w,T_{\text{initial}} \rightarrow T_{\text{final}}}^{\text{eff}}$, column 3 of Table I, to the presence of TC. This is because the spin orientations initially created at T_{initial} after aging for $t_{w,\text{initial}}$ have no relationship to those created when TC occurs. Hence, $t_{w,T_{\text{initial}} \rightarrow T_{\text{final}}}^{\text{eff}}$ represents the growth of $\xi(t_{w,\text{final}}, T_{\text{final}})$ against a background of spin orientations created at T_{initial} after aging for $t_{w,\text{initial}}$. To the extent that TC occurs, the chaotic spin arrangement interferes with the growth of $\xi(t_{w,\text{final}})$, reducing its value of $\xi(t_{w,\text{final}}, T_{\text{final}})$ from what it would have been had there been no TC. If the difference is small, it means that only a small amount of spin orientation after the growth at T_{final} for $t_{w,\text{final}}$ is uncorrelated with the spin orientation created at T_{initial} after $t_{w,\text{initial}}$. That small amount must be the amount of a chaotic state created at T_{final} after the temperature drop.

The relative difference is defined as δ_{TC} , and exhibited in a percentage form as

$$\delta_{\text{TC}} = \frac{t_{\text{R}}^{\text{eff}} - t_{w,T_{\text{initial}} \rightarrow T_{\text{final}}}^{\text{eff}}}{t_{w,T_{\text{initial}} \rightarrow T_{\text{final}}}^{\text{eff}}} \times 100\%. \quad (7)$$

It is plotted as a function of T_{final} in Fig. 4(b). One sees that, even for the smallest temperature drop in our experiments ($\Delta T = T_{\text{initial}} - T_{\text{final}} = 0.05$ K at $T_{\text{final}} = 17.95$

K), the calculated characteristic time, t_R^{eff} , is larger than the measured characteristic time, $t_{w, T_{\text{initial}} \rightarrow T_{\text{final}}}^{\text{eff}}$, by only around 4%. For a slightly larger temperature drop, $\Delta T = 0.10$ K, the difference is larger ($\sim 7\%$) but still small. It is clear from the asymptotic slope of Fig. 4(b) that TC is present, no matter how small ΔT is, which is consistent with the conclusions from numerical simulations [5, 6]. As seen from Fig. 4(b), δ_{TC} increases rapidly as ΔT increases (T_{final} decreases). This rapid increase in TC exhibited in Fig. 4(b) occurs very near the temperature at which Ref. [7] reported the transition to a fully chaotic state, and is consistent with the redictions of the renormalization group [1, 2].

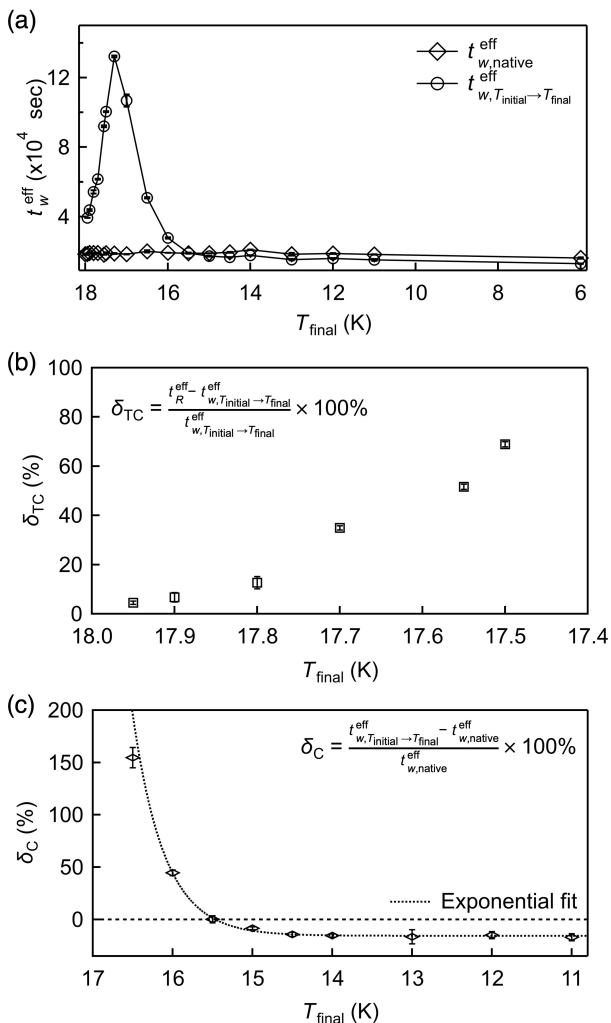


FIG. 4. (a) The measured native effective response time at T_{final} for $t_{w, \text{initial}} = 10^4$ s (diamonds) and the measured effective response time after the $T_{\text{initial}} = 18.00$ K $\rightarrow T_{\text{final}}$ protocol (circles); (b) the difference $\delta_{\text{TC}} = (t_R^{\text{eff}} - t_{w, T_{\text{initial}} \rightarrow T_{\text{final}}}^{\text{eff}}) / t_{w, T_{\text{initial}} \rightarrow T_{\text{final}}}^{\text{eff}} \times 100\%$ at small ΔT s ($\Delta T = T_{\text{initial}} - T_{\text{final}}$); (c) the difference $\delta_C = (t_{w, T_{\text{initial}} \rightarrow T_{\text{final}}}^{\text{eff}} - t_{w, \text{native}}^{\text{eff}}) / t_{w, \text{native}}^{\text{eff}} \times 100\%$ at large ΔT s, with the exponential fit superposed.

The width of $S(t)$ is very broad (examples are exhib-

ited in Appendix A, Figs. 7 and 9). Hence, even though the characteristic times t_R^{eff} are much longer than our laboratory measurement time, the “tail” of their contribution to $S(t)$ is sufficient to contribute to the experimentally measured characteristic time even for $\Delta T = 0.70$ K ($T_{\text{final}} = 17.30$ K). At that temperature, the measured characteristic time $t_{w, T_{\text{initial}} \rightarrow T_{\text{final}}}^{\text{eff}}$ is 13.23×10^4 s while t_R^{eff} is 38.1×10^4 s, somewhat outside of our laboratory measurement time window. The situation begins to reverse when t_R^{eff} begins to move rapidly to much larger values as T_{final} decreases. This is a consequence of both the increase of Δ_{max} with decreasing temperature, and the reduction in temperature T . For example, the measured characteristic effective time $t_{w, T_{\text{initial}} \rightarrow T_{\text{final}}}^{\text{eff}}$, exhibited in Fig. 4(a), begins to decrease as $\Delta T > 0.70$ K for $T_{\text{final}} < 17.30$ K. At $T_{\text{final}} = 17.00$ K, t_R^{eff} is two orders of magnitude larger than the native time. As ΔT continues to increase, the difference increases rapidly, reaching six orders of magnitude at $\Delta T = 3.00$ K ($T_{\text{final}} = 15.00$ K).

The relative difference between $t_{w, T_{\text{initial}} \rightarrow T_{\text{final}}}^{\text{eff}}$ and $t_{w, \text{native}}^{\text{eff}}$ is a measure of how close the system is to a completely chaotic state. We define the relative difference, δ_C , in a percentage form as

$$\delta_C = \frac{t_{w, T_{\text{initial}} \rightarrow T_{\text{final}}}^{\text{eff}} - t_{w, \text{native}}^{\text{eff}}}{t_{w, \text{native}}^{\text{eff}}} \times 100\%. \quad (8)$$

δ_C is exhibited for the lowest values of T_{final} in Fig. 4(c). There are three features that are important. First, δ_C is constant for $T_{\text{final}} \leq 14$ K. This means that the contribution of t_R^{eff} to $S(t)$ is negligible for $T_{\text{final}} \leq 14$ K. The sample is fully chaotic at T_{final} . This is a consequence of the “imprint” of the correlations created at T_{initial} but now completely frozen at T_{final} . The correlation length $\xi(t_{w, \text{final}}, T_{\text{final}})$ grows from nucleation at T_{final} , but its growth is slowed because of interference with the frozen background correlations created by $\xi(t_{w, \text{initial}}, T_{\text{initial}})$. This is consistent with the origins of rejuvenation and memory in [10, 11]. Third, from Table I, the contribution of states at the highest barrier surmounted at T_{initial} must be negligible as ΔT increases. For example, at $T_{\text{final}} = 16.00$ K, $t_R^{\text{eff}} = 1.83 \times 10^8$ s, well beyond the time range of our experiments. Yet, $t_{w, T_{\text{initial}} \rightarrow T_{\text{final}}}^{\text{eff}}$ is still larger than $t_{w, \text{native}}^{\text{eff}}$ even for this very large value of t_R^{eff} . This must arise from free energy barriers smaller than $\Delta_{\text{max}}(t_{w, \text{initial}}, T_{\text{initial}})$. However, at T_{final} , they have grown sufficiently (because of the consequences of Fig. 2) that their effective time scale is comparable to our measurement time. Because of ultrametric symmetry (see Sec. II), their number of states must be exponentially smaller than the number of states at $\Delta_{\text{max}}(t_{w, \text{initial}}, T_{\text{initial}})$. Thus, their contribution should fall off exponentially with increasing ΔT (lower T_{final}). This predicted behavior is exhibited in the exponential fit of Fig. 4(c).

Complementary experiments were carried out at $T_{\text{initial}} = 16.00$ K instead of $T_{\text{initial}} = 18.00$ K to check if our analysis is consistent with the accepted length

TABLE II. Listing of measured and calculated effective response times for $T_{\text{initial}} = 16.00$ K at different T_{final} .

T (K)	$t_{w,\text{native}}^{\text{eff}} (\times 10^4 \text{ s})$	$t_{w,T_{\text{initial}} \rightarrow T_{\text{final}}}^{\text{eff}} (\times 10^4 \text{ s})$	$t_{\text{R}}^{\text{eff}} (\text{s})$	ξ/a_0
16.00	1.92 ± 0.01	-	-	7.258
15.50	1.90 ± 0.03	9.70 ± 0.08	1.37×10^5	6.695
15.00	1.89 ± 0.01	12.37 ± 0.13	8.33×10^5	6.183
14.50	1.94 ± 0.03	7.33 ± 0.11	6.45×10^6	5.717
14.00	2.09 ± 0.01	3.36 ± 0.11	5.89×10^7	5.384
13.00	1.84 ± 0.07	1.98 ± 0.11	8.23×10^9	4.625
12.00	1.87 ± 0.03	1.71 ± 0.04	2.62×10^{12}	4.052
11.00	1.82 ± 0.01	1.49 ± 0.02	2.38×10^{15}	3.558

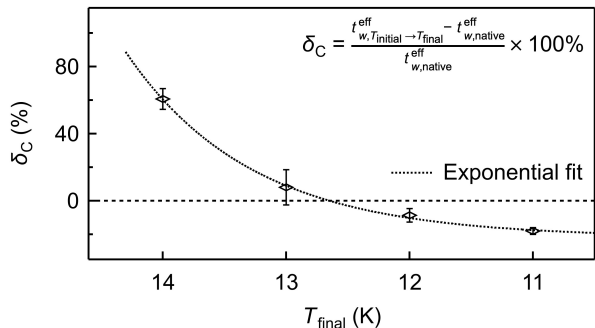
scale dependence of TC. Table II lists our results for $T_{\text{initial}} = 16.00$ K in the same format as in Table I for $T_{\text{initial}} = 18.00$ K. First, for $\Delta T = 0.50$ K, the calculated $t_{\text{R}}^{\text{eff}}$ is smaller for $T_{\text{initial}} = 16.00$ K (1.37×10^5 s as compared to 1.70×10^5 s) because, at the lower temperature, the growth of the correlation length is slower, resulting in a smaller $\Delta_{\text{max}}(t_{w,\text{initial}}, T_{\text{initial}})$ for $T_{\text{initial}} = 16.00$ K as compared to $T_{\text{initial}} = 18.00$ K. Concomitantly, $t_{w,T_{\text{initial}} \rightarrow T_{\text{final}}}^{\text{eff}} = 9.70 \times 10^4$ s for $T_{\text{initial}} = 16.00$ K is less than that of 10.04×10^4 s for $T_{\text{initial}} = 18.00$ K.

When we compare δ_{TC} at the same values of ΔT for the two initial values of T_{initial} , we are comparing the differences in the amount of TC. We find, expressed as percentages in analogy with Fig. 4(b), $\delta_{\text{TC}} = 41 \pm 1\%$ ($T_{\text{initial}} = 16.00$ K) vs $\delta_{\text{TC}} = 69 \pm 1\%$ ($T_{\text{initial}} = 18.00$ K), or a lesser amount of TC for $T_{\text{initial}} = 16.00$ K by $28 \pm 2\%$. Remembering that TC is related to a comparison between length scales for the correlation length and the equivalent length for chaos [2], we can make use of the values for ξ/a_0 in the fifth columns of Tables I and II. The difference of ξ/a_0 between $T = 18.00$ K and $T = 16.00$ K is $9.715 - 7.258 = 2.457$, or about 25% of the former. Because the chaos length scale exponent $1/\zeta \sim 1.0$ (Appendix B of [7]) this difference is approximately the difference in the amount of TC between the two initial temperatures. The consistency of each of these estimates lends further credence to the TC interpretation of our experiments.

A further comparison of the results for $T_{\text{initial}} = 16.00$ K with $T_{\text{initial}} = 18.00$ K, but now at larger ΔT , illustrates the approach to complete chaos through δ_{C} . Expressed as a percentage, Table III compares δ_{C} for the two values of T_{initial} . The difference δ_{C} for $T_{\text{initial}} = 16.00$ K is plotted in Fig. 5. As before, the approach to a completely chaotic state can be fitted to an exponential (the dotted curve in Fig. 5) because of the ultrametric distribution of states. As ΔT increases from $T_{\text{initial}} = 16.00$ K, the approach to a purely chaotic state is slower than that at $T_{\text{initial}} = 18.00$ K. This is because $\xi/a_0(T = 16.00$ K) is smaller than $\xi/a_0(T = 18.00$ K) (see Tables I and II), requiring a larger ΔT for crossover to chaos [2]. This is seen quantitatively in Table III where it takes a larger ΔT for $t_{w,T_{\text{initial}} \rightarrow T_{\text{final}}}^{\text{eff}}$ to reach $t_{w,\text{native}}^{\text{eff}}$ for $T_{\text{initial}} = 16.00$ K as compared to that for $T_{\text{initial}} = 18.00$ K.

TABLE III. Listing of the percent difference $\delta_{\text{C}} = (t_{w,T_{\text{initial}} \rightarrow T_{\text{final}}}^{\text{eff}} - t_{w,\text{native}}^{\text{eff}})/t_{w,\text{native}}^{\text{eff}} \times 100\%$ at different ΔT 's between $T_{\text{initial}} = 18.00$ K and $T_{\text{initial}} = 16.00$ K.

ΔT (K)	T_{initial} (K)	T_{final} (K)	δ_{C} (%)
1.00	18.00	17.00	480 ± 23
	16.00	15.00	554 ± 8
1.50	18.00	16.50	155 ± 10
	16.00	14.50	278 ± 11
2.00	18.00	16.00	45 ± 3
	16.00	14.00	61 ± 6
3.00	18.00	15.00	-8 ± 1
	16.00	13.00	8 ± 11
4.00	18.00	14.00	-15 ± 2
	16.00	12.00	-9 ± 4
5.00	18.00	13.00	-17 ± 7
	16.00	11.00	-18 ± 2

FIG. 5. The percent difference $\delta_{\text{C}} = (t_{w,T_{\text{initial}} \rightarrow T_{\text{final}}}^{\text{eff}} - t_{w,\text{native}}^{\text{eff}})/t_{w,\text{native}}^{\text{eff}} \times 100\%$ between the measured effective response time after the $T_{\text{initial}} \rightarrow T_{\text{final}}$ protocol and the measured native effective response time at large ΔT 's.

IV. SUMMARY

Our experiments display the growth of TC in spin glasses over the full range of temperature change. The magnitude of TC to spin glass dynamics is small at small ΔT . As the temperature change increases, TC becomes more significant, increasing rapidly in the vicinity of the crossover ΔT predicted from renormalization group methods [2] and seen experimentally [7, 9]. Upon further

increase in ΔT , the system rapidly approaches a fully chaotic state. We believe this set of experiments lays a firm basis for the onset of TC in spin glass dynamics, and confirms the predictions of simulations that find “... a complete reorganization of the equilibrium configurations [takes place] by the slightest change in temperature.”

ACKNOWLEDGMENTS

We are pleased to acknowledge the assistance of the Janus II Collaboration during the progress of our experiments, and the advice in particular of Professor Victor Martin-Mayor. We also acknowledge the suggestions for our data analysis from Professor E. Dan Dahlberg and Dr. J. Freedberg. The use of the single CuMn crystal, grown by Dr. D.L. Schlagel at Ames Laboratory, was crucial for our investigation. This work was supported by the U.S. Department of Energy, Office of Science, Basic Energy Sciences, Division of Materials Science and Engineering, under Award No. DE-SC0013599. Dr. D.L. Schlagel’s work was performed at Ames Laboratory, which is operated for the U.S. Department of Energy by Iowa State University under Contract No. DE-AC02-07CH11358. H. Li acknowledges the partial support by the National Science Foundation through the Center for Dynamics and Control of Materials: an NSF MRSEC under Cooperative Agreement No. DMR-2308817.

Appendix A: Determination of the $S(t)$ peak

As shown in Eq. (1), the relaxation function $S(t)$ is the first derivative of the magnetization with respect to the natural logarithm of time. Therefore, the noise in the magnetization measurements makes it impractical to locate the $S(t)$ peak by using raw data. In our analysis, we have used a log-normal distribution function to obtain a smooth approximation to the raw data.

$$M_{\text{ZFC}}(t, t_w; T) = M_0 + Ae^{-[\ln(t/t_0)/w]^2} \quad (\text{A1})$$

The approximation from Eq. (A1) is unable to reproduce the shape of the $M-t$ curve in its full range. Taking the native measurement at $T_{\text{final}} = 16.50$ K as an example, the full-range fit of the raw data to Eq. (A1) in Fig. 6 gives an $S(t)$ peak at 2.56×10^4 s in Fig. 7. However, the difference between the fit result and the raw data in the vicinity of the $S(t)$ peak is so large that the position of the $S(t)$ maximum is not reliable.

Considering that we are only interested in the position of the maximum of the $S(t)$ curve, a shorter range fit around the expected $S(t)$ peak in Fig. 8 is a more attractive approach. For example, we find the $S(t)$ peak position from a shorter-range fit to be 2.00×10^4 s as shown in Fig. 9. The difference between the fit result and the raw data near $t = 2.00 \times 10^4$ s indicates a good fit and thus a reliable $S(t)$ peak position.

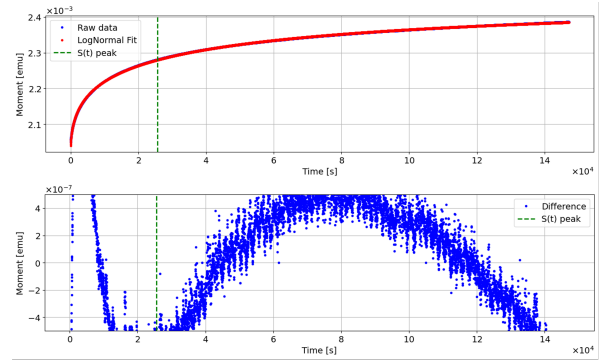


FIG. 6. (Color online) The full-range fit of the native measurement data at $T_{\text{final}} = 16.50$ K to Eq. (A1). The upper panel shows the fit result and the lower panel shows the difference between the fit result and the raw data. The extracted peak position is 2.56×10^4 s as indicated by the green dash line, where the difference between the fit and raw data is largest.

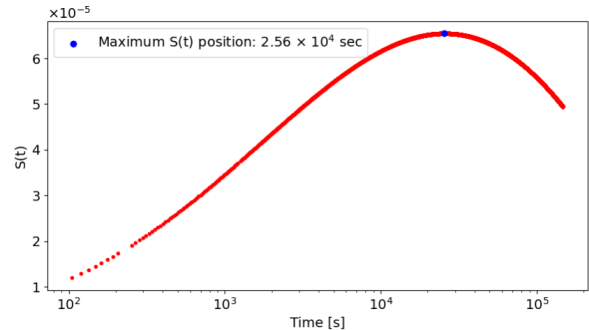


FIG. 7. (Color online) $S(t)$ from the full-range fit of the native measurement at $T_{\text{final}} = 16.50$ K.

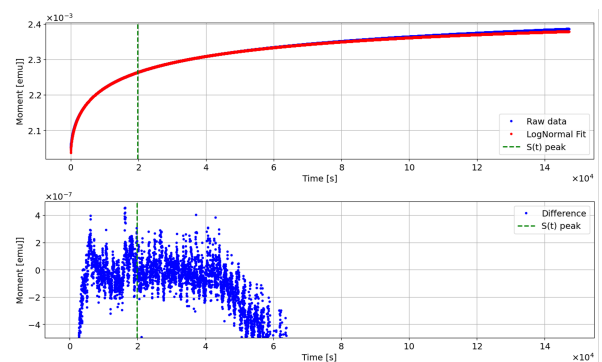


FIG. 8. (Color online) The shorter-range fit of the native measurement data at $T_{\text{final}} = 16.50$ K to Eq. (A1). The upper panel shows the fit result and the lower panel shows the difference between the fit result and the raw data. The peak position is at 1.98×10^4 s as indicated by the green dash line, where the difference between the fit and raw data is smallest.

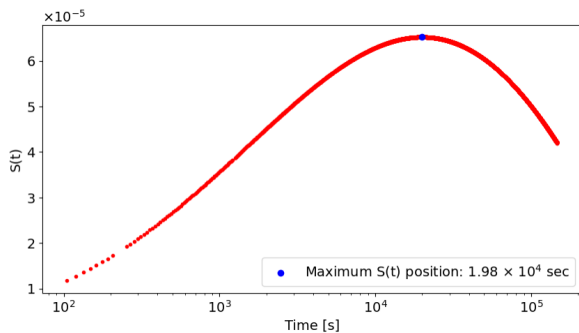


FIG. 9. (Color online) $S(t)$ from the short-range fit of the native measurement at $T_{\text{final}} = 16.50$ K.

In the short-range fit, the size and position of the fitting range could affect the position of the $S(t)$ peak. For that reason, we take the center of the shorter-range fit to be at the expected position of the $S(t)$ peak. The fitting range should be large enough that it covers the earlier period where $M_{\text{ZFC}}(t, t_w; T)$ increases relatively rapidly, so that, as much as possible, the shape information of the $M - t$ curve is preserved. We utilize a scanning protocol to determine the fitting range position. The $T_{\text{initial}} \rightarrow T_{\text{final}}$ measurement at $T_{\text{final}} = 17.50$ K, as described below, is an example.

(1) We first fit the raw data to Eq. (A1) to the full range to get an estimate of the position of the $S(t)$ peak is. At $T_{\text{final}} = 17.50$ K, the full-range fit results in an $S(t)$ peak at 9.67×10^4 s as shown in Fig. 10, the 5437th point in our raw data.

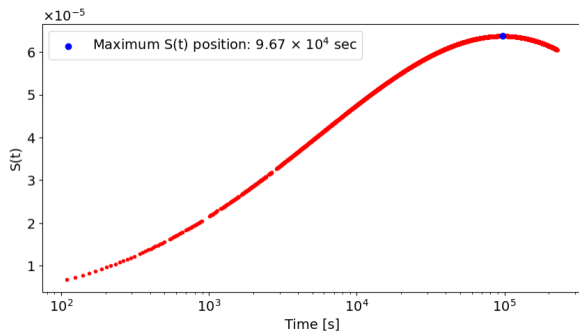


FIG. 10. (Color online) $S(t)$ from the full-range fit of the $T_{\text{initial}} \rightarrow T_{\text{final}}$ measurement at $T_{\text{final}} = 17.50$ K.

(2) We then choose the size of the fitting range for the shorter-range fit. In our measurements, the time interval between each data point is approximately 15 s. Typically a 2001-point fitting range is large enough for our native measurement, while the $T_{\text{initial}} \rightarrow T_{\text{final}}$ measurements require a 3001-point to 6001-point fitting range depending on the $S(t)$ peak position. In our analysis, we found that a reasonable change (5%) in the fitting range size still provides us with the similar results for the $S(t)$ peak position within the error bars. For the $T_{\text{initial}} \rightarrow T_{\text{final}}$ measurement at $T_{\text{final}} = 17.50$ K discussed here, we used

a 6001-point fitting range. We scanned the 6001-point fitting range across our raw data from a fitting range centered at the 4800th point, and then to the fitting range centered at 6200th point with a 35-point interval. The $S(t)$ peak position and its data point index are shown in Fig. 11. By comparing the center of the fitting range and the index of the corresponding $S(t)$ peak position, we found that the center of the fitting range should occur near the 5670th point.

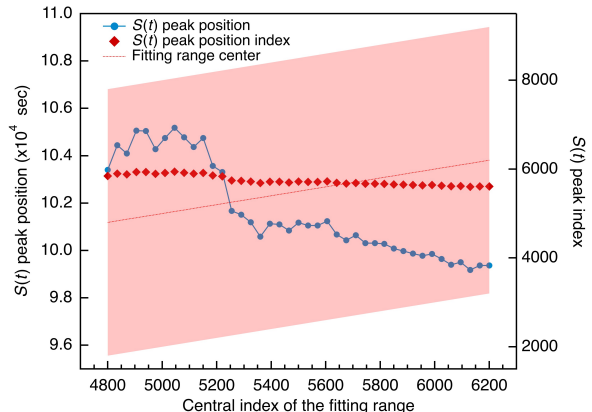


FIG. 11. (Color Online) The short-range fit scanning results of the $T_{\text{initial}} \rightarrow T_{\text{final}}$ measurement at $T_{\text{final}} = 17.50$ K. The blue dots show the $S(t)$ position and the red diamonds show their corresponding index in the raw data. The red shaded region shows the fitting range, with the center of the fitting range depicted by the red dashed line.

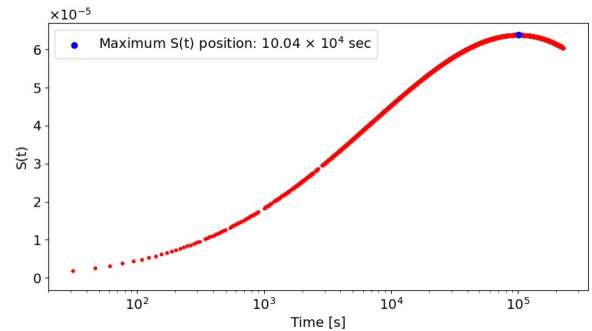


FIG. 12. (Color Online) $S(t)$ from the 6001-point fit of the $T_{\text{initial}} \rightarrow T_{\text{final}}$ measurement at $T_{\text{final}} = 17.50$ K, with the $S(t)$ peak position being the center of the fitting range.

(3) We take an iterative process to determine the final position of the fitting range. As discussed in (2), the fitting range center should be placed near the 5670th point. Therefore, we started the iterative process below with the fitting range center being the 5670th point.

(a) We started with a fitting range from the 2670th point to the 8670th point with its center being the 5670th point. We obtained a $S(t)$ peak of 10.04×10^4 s at the 5674th point in our raw data.

(b) We then set the 5674th point, the $S(t)$ peak index

TABLE IV. Listing of measured native effective response time and $T_{\text{initial}} \rightarrow T_{\text{final}}$ effective response time for the temperature $T_{\text{final}} = 17.80$ K at different applied magnetic fields.

$T_{\text{initial}}(\text{K})$	$T_{\text{final}}(\text{K})$	$H(\text{Oe})$	$t_{\text{w,native}}^{\text{eff}}(\times 10^4 \text{ s})$	$t_{\text{w},T_{\text{initial}} \rightarrow T_{\text{final}}}^{\text{eff}}(\times 10^4 \text{ s})$
18.00	17.80	50	1.96 ± 0.01	5.42 ± 0.08
		100	1.90 ± 0.03	5.42 ± 0.10

obtained in (a), to be the center of our new fitting range from the 2674th point to the 8674th point. We obtained a $S(t)$ peak of 10.04×10^4 s at the 5674th point in our raw data. With the fitting range center being exactly at the $S(t)$ peak position, we consider it to be our final result for the position of the peak in $S(t)$ peak position as exhibited in Fig. 12.

By using a shorter-range fit of the raw data to Eq. (A1) with the scanning protocol explained above, we are able to obtain the characteristic time from the $S(t)$ peak position at different temperatures with much higher accuracy than has heretofore been reported in the literature. The entries in Table I and Table II of the main text are the

results from this process.

Appendix B: The magnetic linearity

To investigate the magnetic linearity of our results, we conducted measurements for the native effective response time, $t_{\text{w,native}}^{\text{eff}}$, and the $T_{\text{initial}} \rightarrow T_{\text{final}}$ effective response time, $t_{\text{w},T_{\text{initial}} \rightarrow T_{\text{final}}}^{\text{eff}}$, with $T_{\text{initial}} = 18.00$ K and $T_{\text{final}} = 17.80$ K under an applied magnetic field of 50 Oe. The results obtained at 50 Oe are listed in Table IV with the results obtained at 100 Oe, and the magnetic field effect on both effective response times is negligible in our analysis and discussions.

-
- [1] S. R. McKay, A. N. Berker, and S. Kirkpatrick, Phys. Rev. Lett. **48**, 767 (1982).
 - [2] A. J. Bray and M. A. Moore, Phys. Rev. Lett. **58**, 57 (1987).
 - [3] D. S. Fisher and D. A. Huse, Phys. Rev. Lett. **56**, 1601 (1986).
 - [4] D. S. Fisher and D. A. Huse, Phys. Rev. B **38**, 386 (1988).
 - [5] L. A. Fernandez, V. Martin-Mayor, G. Parisi, and B. Seoane, Europhysics Letters **103**, 67003 (2013).
 - [6] M. Baity-Jesi, E. Calore, A. Cruz, L. A. Fernandez, J. Gil-Narvion, I. Gonzalez-Adalid Pearnin, A. Gordillo-Guerrero, D. Iñiguez, A. Maiorano, E. Marinari, V. Martin-Mayor, J. Moreno-Gordo, A. Muñoz-Sudupe, D. Navarro, I. Paga, G. Parisi, S. Perez-Gaviró, F. Ricci-Tersenghi, J. J. Ruiz-Lorenzo, S. F. Schifano, B. Seoane, A. Tarancon, R. Tripiccione, and D. Yllanes, Communications Physics **4**, 74 (2021).
 - [7] Q. Zhai, R. L. Orbach, and D. L. Schlagel, Phys. Rev. B **105**, 014434 (2022).
 - [8] P. E. Jönsson, H. Yoshino, and P. Nordblad, Phys. Rev. Lett. **89**, 097201 (2002).
 - [9] S. Guchhait and R. L. Orbach, Phys. Rev. B **92**, 214418 (2015).
 - [10] J. Freedberg, W. J. Meese, J. He, D. L. Schlagel, E. D. Dahlberg, and R. L. Orbach, Phys. Rev. B **110**, L060411 (2024).
 - [11] I. Paga, J. He, M. Baity-Jesi, E. Calore, A. Cruz, L. A. Fernandez, J. M. Gil-Narvion, I. G.-A. Pearnin, A. Gordillo-Guerrero, D. Iñiguez, A. Maiorano, E. Marinari, V. Martin-Mayor, J. Moreno-Gordo, A. M. Sudupe, D. Navarro, R. L. Orbach, G. Parisi, S. Perez-Gaviró, F. Ricci-Tersenghi, J. J. Ruiz-Lorenzo, S. F. Schifano, D. L. Schlagel, B. Seoane, A. Tarancon, and D. Yllanes, Phys. Rev. Lett., in press (2024).
 - [12] P. Sibani, J. C. Schön, P. Salamon, and J.-O. Andersson, Europhysics Letters **22**, 479 (1993).
 - [13] J. Kisker, L. Santen, M. Schreckenberg, and H. Rieger, Phys. Rev. B **53**, 6418 (1996).
 - [14] E. Marinari, G. Parisi, J. Ruiz-Lorenzo, and F. Ritort, Phys. Rev. Lett. **76**, 843 (1996).
 - [15] P. Nordblad, P. Svedlindh, L. Lundgren, and L. Sandlund, Phys. Rev. B **33**, 645 (1986).
 - [16] Y. G. Joh, R. Orbach, G. G. Wood, J. Hammann, and E. Vincent, Phys. Rev. Lett. **82**, 438 (1999).
 - [17] P. Refregier, E. Vincent, J. Hammann, and M. Ocio, J. Phys. France **48**, 1533 (1987).
 - [18] M. Lederman, R. Orbach, J. M. Hammann, M. Ocio, and E. Vincent, Phys. Rev. B **44**, 7403 (1991).
 - [19] J. Hammann, M. Lederman, M. Ocio, R. Orbach, and E. Vincent, Physica A Statistical Mechanics and its Applications **185**, 278 (1992).
 - [20] G. Parisi, Phys. Rev. Lett. **43**, 1754 (1979).
 - [21] G. Parisi, Phys. Rev. Lett. **50**, 1946 (1983).
 - [22] S. Kirkpatrick and D. Sherrington, Phys. Rev. B **17**, 4384 (1978).
 - [23] E. Vincent, J. Hammann, and M. Ocio, J. Stat. Phys. **135**, 1105 (2009).